

The European Large Area *ISO* Survey (ELAIS): The Final Band-merged Catalogue

M.Rowan-Robinson¹, C.Lari⁸, I.Perez-Fournon¹¹, E.A.Gonzalez-Solares⁵,
 F.La Franca⁷, M.Vaccari⁴, S.Oliver⁹, C.Gruppioni², P.Ciliegi²,
 P.Héraudeau⁶, S.Serjeant¹⁰, A.Efstathiou³, T.Babbedge¹, I.Matute⁷,
 F. Pozzi², A.Franceschini⁴, P.Vaisanen¹²,
 A.Afonso-Luis¹¹, D.M. Alexander⁵, O. Almaini¹³, A.C. Baker¹⁴, S.Basilakos¹⁷,
 M. Barden¹⁶, C.del Burgo³³, I. Bellas-Velidis¹⁷, F. Cabrera-Guerra¹⁰,
 R. Carballo^{15,18}, C.J. Cesarsky¹⁹, D.L. Clements¹, H. Crockett¹, L. Danese²⁰,
 A. Dapergolas¹⁶, B. Drolias¹, N. Eaton¹, E. Egami²¹, D. Elbaz¹⁹, D. Fadda¹⁰,
 M. Fox¹, R. Genzel¹⁶, P. Goldschmidt¹, J.I.Gonzalez-Serrano^{15,18}, M. Graham¹,
 G. L. Granato⁴, E.Hatziminaoglou¹¹, U. Herbstmeier²², M. Joshi¹, E. Kontizas¹⁷,
 M. Kontizas²³, J.K. Kotilainen²⁴, D. Kunze¹⁶, A. Lawrence¹³, D. Lemke²²,
 M.J.D. Linden-Vørnle^{25,26}, R.G. Mann¹³, I. Márquez²⁷, J. Masegosa²⁷,
 R.G. McMahon⁵, G. Miley²⁸, V. Missoulis¹, B. Mobasher²⁹, T. Morel³⁵,
 H. Nørgaard-Nielsen²⁶, A. Omont³¹, P. Papadopoulos²⁸, J-L. Puget³¹, D. Rigopoulou³⁴,
 B. Rocca-Volmerange³⁰, N.Sedgwick¹⁰, L. Silva²⁰, T. Sumner¹, C. Surace¹,
 B.Vila-Vilaro,²¹, P. van der Werf²⁸, A. Verma¹⁶, L. Vigroux¹⁹, M. Villar-Martin³¹,
 C.J. Willott³²

¹ Astrophysics Group, Blackett Laboratory, Imperial College of Science Technology & Medicine (ICSTM), Prince Consort Rd., London SW7 2BZ, ² Osservatorio Astronomico di Bologna, via Ranzani 1, 40127 Bologna, Italy

³ Dept of Computer Science and Engineering, Cyprus College, 6 Diogenes St, Engomi, 1516 Nicosia, Cyprus

⁴ Dipartimento di Astronomia, Università di Padova, Vicolo Osservatorio 5, I-35122 Padova, Italy

⁵ Institute of Astronomy, Madingley Road, Cambridge, CB3 0HA, ⁶ Kapteyn Astronomical Institute, Postbus 800, 9700 AV Groningen, Netherlands, ⁷ Dipartimento di Fisica, Università degli Studi "Roma TRE" Via della Vasca Navale 84, I-00146, Roma, Italy, ⁸ Institute di Radio Astronomy, Bologna, Italy

⁹ Astronomy Centre, Department of Physics & Astronomy, University of Sussex, Brighton, BN1 9QJ, UK

¹⁰ Centre for Astrophysics and Planetary Science, School of Physical Sciences, University of Kent, Canterbury, Kent CT2 7HR, UK

¹¹ Instituto de Astrofísica de Canarias, C/ Via Lactea, s/n, 38200 La Laguna, S/C de Tenerife, Spain

¹² European Southern Observatory, Casilla 19001, Santiago, Chile, ¹³ Institute for Astronomy, University of Edinburgh, Royal Observatory, Blackford Hill, Edinburgh EH9 3HJ, ¹⁴ Dept of Physics & Astronomy, Cardiff University, PO Box 913, Wales CF24 3YB

¹⁵ Instituto de Física de Cantabria (Consejo Superior de Investigaciones Científicas - Universidad de Cantabria, 39005 Santander, Spain, ¹⁶ Max-Planck-Institut für extraterrestrische Physik, Postfach 1603, 85740 Garching, Germany

¹⁷ National Observatory of Athens, Astronomical Institute, PO Box 20048, GR-11810, Greece

¹⁸ Departamento de Física Moderna, Universidad de Cantabria, 39005 Santander, Spain

¹⁹ CEA / SACLAY, 91191 Gif sur Yvette cedex, France, ²⁰ SISSA, International School for Advanced Studies, Via Beirut 2-4, 34014 Trieste, Italy, ²¹ Steward Observatory, University of Arizona, 933 North Cherry Avenue, Tucson, AZ 85721-0065

²² Max-Planck-Institut für Astronomie, Königstuhl (MPIA) 17, D-69117, Heidelberg, Germany

²³ Section of Astrophysics, Astronomy & Mechanics, Dept. of Physics, University of Athens, Panepistimiopolis, GR-15783, Zografos, Greece, ²⁴ Tuorla Observatory, University of Turku, Väisäläntie 20, FIN-21500 Piikkiö, Finland

²⁵ Niels Bohr Institute for Astronomy, Physics and Geophysics, Astronomical Observatory, Juliane Maries Vej 30, DK-2100 Copenhagen Ø, Denmark, ²⁶ Danish Space Research Institute, Juliane Maries Vej 30, DK-2100 Copenhagen Ø, Denmark

²⁷ Instituto de Astrofísica de Andalucía, CSIC, Apartado 3004, E-18080 Granada, Spain.

²⁸ Leiden Observatory, P.O.Box 9513, NL-2300 RA Leiden, Netherlands, ²⁹ Space Telescope Science Institute, Baltimore, FA, USA

³⁰ Institut d'Astrophysique de Paris, 98bis Boulevard Arago, F 75014 Paris, France

³¹ Institut d'Astrophysique Spatiale (IAS), Bâtiment 121, Université Paris XI, 91405 Orsay cedex, France

³² Toronto, Canada, ³³ ESTEC, Keplerlaan 1, Postbus 299, 2200 AG Nordwijk, Netherlands

³⁴ Physics Dept., University of Oxford, Denys Wilkinson Building, Keble Rd, Oxford OX1 3RH, UK

³⁵ Osservatorio Astronomico di Palermo G.S.Vaiana, Piazza del Parlamento 1, I-90134 Palermo, Italy

ABSTRACT

We present the final band-merged ELAIS catalogue at 6.7, 15, 90, and 175 μm , and the associated data at u,g,r,i,z,J,H,K, and 20cm. The origin of the survey, infrared and radio observations, data-reduction and optical identifications are briefly reviewed, and a summary of the area covered, and completeness limit for each infrared band is given. A detailed discussion of the band-merging and optical association strategy is given. The total catalogues consists of 2860 sources. 22 % of the 15 μm sources and 75 % of the 6.7 μm sources are stars. For extragalactic sources observed in 3 or more infrared bands, colour-colour diagrams are presented and discussed in terms of the contributing infrared populations. Spectral energy distributions are shown for selected sources and compared with cirrus, M82 and Arp220 starburst, and AGN dust torus models.

Spectroscopic redshifts are tabulated, where available. For the N1 and N2 areas, the INT ugriz Wide Field Survey, permits photometric redshifts to be estimated for galaxies and quasars. These agree well with the spectroscopic redshifts, within the uncertainty of the photometric method ($\sim 10\%$ in $(1+z)$). The redshift distribution is given for selected ELAIS bands and colour-redshift diagrams are discussed.

There is a high proportion of ultraluminous infrared galaxies (1-1000 μm luminosity $L_{\text{ir}} > 12.22$) in the ELAIS Catalogue ($> 10\%$ of 15 μm sources), many with Arp220-like colours. 8 % of the 15 μm sources are genuine optically blank fields: these must have high infrared-to-optical ratios and probably have $z > 0.2$, so are high luminosity dusty starbursts or Type 2 AGN. 10 hyperluminous infrared galaxies ($L_{\text{ir}} > 13.22$) are found in the survey. The large numbers of ultraluminous galaxies imply very strong evolution in the star-formation rate between $z = 0$ and 1.

Key words: infrared: galaxies - galaxies: evolution - star:formation - galaxies: starburst - cosmology: observations

1 INTRODUCTION

The European Large Area *ISO* Survey (ELAIS) was originally proposed in response to the first Infrared Space Observatory (*ISO*) call for open time proposals in 1995 by M.Rowan-Robinson and 11 co-investigators from 9 institutions (Rowan-Robinson et al 1999). Subsequently the collaboration has grown to a total of 76 investigators from 30 European institutions. The original concept was for a survey of 12 sq deg of sky at wavelengths of 15 and 90 μm . Subsequent awards of observing time allowed the survey to be extended to 6.7 μm and (in collaboration with the FIRBACK team led by J.-L.Puget) 175 μm . The ELAIS areas were also surveyed at 20 cm with the VLA and the AT.

The survey goals, selection of survey areas, and details of the *ISO* observations, were described by Oliver et al (2000), and a preliminary analysis of the 6.7 and 15 μm data was reported by Serjeant et al (2000) and of the 90 μm data by Efstathiou et al (2000). A new method of reduction of the 15 μm data, which incorporates a physical models of cosmic ray and transient effects, was given by Lari et al (2001), and a first application of this to the ELAIS S1 area was described by Gruppioni et al (2001). The final 15

μm reduction of the S1 area is reported by Lari et al (2003), of the S2 area by Pozzi et al (2003) and of the N1, N2 and N3 areas by Vaccari et al (2003) (see below for explanation of survey areas). The final reduction of the 90 μm data is reported by Héraudeau et al (2003) and of the FIRBACK-ELAIS 175 μm data by Dole et al (2002). The reduction and analysis of the 20 cm data was described by Ciliegi et al (1999) for N1, N2 and N3, and by Gruppioni et al (1999) for S1 and S2.

Associated with the ELAIS survey there has also been an extensive program of ground-based optical and near-infrared imaging and spectroscopy. The optical and spectroscopic follow-up of the S1 area has been presented by La Franca et al (2003), of the S2 area by Pozzi et al (2003), and of the N1 and N2 areas by Heraudeau et al (1999), Vaisanen et al (2002), Gonzalez-Solares et al (2003), Perez-Fournon et al (2003), Serjeant et al (2003), Verma et al (2003) and Afonso-Luis et al (2003).

Deeper surveys at 6.7 and 15 μm were also carried out by a subset of the ELAIS consortium in HDF-N (Serjeant et al 1997, Goldschmidt et al 1997, Oliver et al 1997, Mann et al 1997, Rowan-Robinson et al 1997) and in HDF-S (Oliver et al 2002, Mann et al 2002).

X-ray surveys have also been carried out in several ELAIS areas. Alexander et al (2001) reported Beppo-Sax observations over a large fraction of S1. Manners et al (2003) have reported Chandra observations in the central regions of N1 and N2, and some interpretation of these observations has been given by Willott et al (2003). ROSAT data were compared with the ELAIS Preliminary Catalogue by Basilakos et al (2002).

The present paper reviews the parameters of the ELAIS survey, gives a detailed account of the merging of the different individual wavelength surveys to generate a final catalogue, and discusses the populations present in the survey through colour-colour and colour-redshift diagrams, and spectral energy distributions.

2 QUALITY OF THE CONSTITUENT INFRARED CATALOGUES

The separate wavebands making up the ELAIS survey each comprise an independent survey and are discussed in separate papers. The present paper does not replace these analyses but pulls together those aspects which emerge from band-merging the surveys. For detailed discussion and analysis of the ELAIS sources, it is essential to refer back to these analyses of the individual constituent surveys. Table 1 defines the survey areas, wavelengths, characteristic depth, and source-densities.

The calibration, completeness and reliability of the ELAIS $15\ \mu\text{m}$ survey final analysis has been discussed by Lari et al (2001, 2003), Gruppioni et al (2001) and Vaccari et al (2003). The final derived conversion factor from *ISO* instrumental units (ADU) to mJy of 1.098 ± 0.012 is consistent with that derived for the Preliminary Analysis (PA) catalogue by Vaisanen et al (2002), using J and K observations of stars, of 1.05, but disagrees with that derived by Serjeant et al (2000), 1.75, based on *IRAS* sources in common (see section 3). Figure 1 shows a plot of the final $15\ \mu\text{m}$ flux, S_{15} , versus the PA flux (in ADU) (Babbedge 2004). The Final Analysis catalogue goes significantly deeper than the PA catalogue, but almost all PA sources are found to be real.

For the $6.7\ \mu\text{m}$ survey we decided that (i) on the basis of the Vaisanen et al (2002) analysis the quality of the Preliminary Analysis was adequate, (ii) that although application of the Lari et al. (2001) analysis method would lead to improved reliability and deeper source extraction, the scientific returns would not justify the resources required, especially since the main ELAIS areas are to be surveyed by the SIRTF-SWIRE survey at $8\ \mu\text{m}$ (Lonsdale et al. 2003). The $6.7\ \mu\text{m}$ PA catalogue has duplicate entries where different rasters observed the same part of the sky and only the entry with lowest noise was included.

The calibration, completeness and reliability of

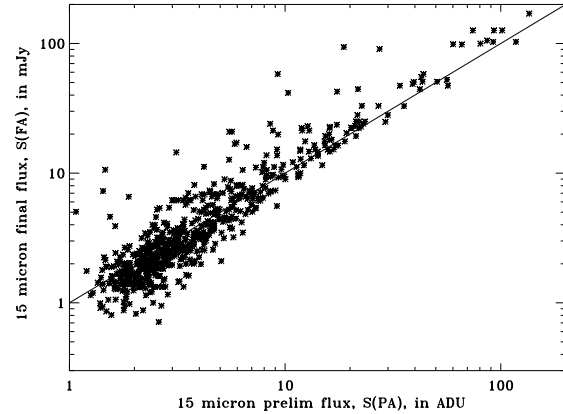


Figure 1. Comparison of Final Analysis $15\ \mu\text{m}$ flux (mJy) (Lari et al 2003, Vaccari et al 2003) with Preliminary Analysis $15\ \mu\text{m}$ fluxes (ADU) (Serjeant et al 2000). The line corresponds to equal fluxes.

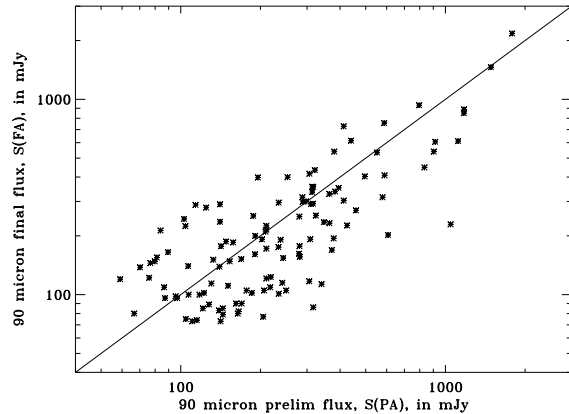


Figure 2. Comparison of Final Analysis $90\ \mu\text{m}$ flux (mJy) (Heraudeau et al. 2003) with Preliminary Analysis $90\ \mu\text{m}$ fluxes (Efstathiou et al 2000).

the ELAIS $90\ \mu\text{m}$ survey final analysis has been discussed by Heraudeau et al (2003). Figure 2 shows a plot of the final $90\ \mu\text{m}$ flux, S_{90} , versus the PA flux (Babbedge 2004). Again, most of the PA sources are confirmed.

The $175\ \mu\text{m}$ data analysis and identifications have been discussed by Dole et al (2002). A 5σ sensitivity of 223 mJy was achieved.

3 FINAL BAND-MERGED CATALOGUE

3.1 Band-merging

We have proceeded with the band-merging of the multi-wavelength ELAIS catalogues in a sequential way, taking into account the different positional accuracies of the component catalogues. The 1σ po-

Table 1. Summary of survey wavelengths, areas and numbers of sources, characteristic depth, source-densities

Name	RA	Dec	6.7	15	90	175 μ m
N1	16 ^h 10 ^m 01 ^s	+54°30'36"		2.67/490	2.56/151	2/103 (sq deg/no. of sources)
N2	16 36 58	+41 15 43	2.67/628	2.67/566	2.67/174	1/55
N3	14 29 06	+33 06 00	1.32/189	0.88/131	1.76/119	
S1	00 34 44	-43 28 12	1.76/304	3.96/317	3.96/226	
S2	05 02 24	-30 35 55	0.12/40	0.12/43	0.11/5	
total area/number		5.86/1161	10.3/1546	11.06/674	3.0/158	sq deg/no. of sources
characteristic depth		1.0	0.7	70	223 mJy	
source-density		200	150	61	53 per sq deg	

sitional uncertainties at 15 μ m and 20cm have been estimated to be $\sim 1''$ (Lari et al 2003, Vaccari et al 2003, Gonzalez-Solares et al 2003, Ciliegi et al 1999, Gruppioni et al 1999), so sources at these wavelengths can be very reliably associated with optical counterparts, down to at least $r \sim 23$ mag. We therefore first separately identify the 15 μ m and 20 cm catalogues with optical sources, as discussed by Gonzalez-Solares et al (2003). The 15 μ m and 20 cm sources are then merged on the basis of their optical positions, using a search radius of 2''. The percentages of 15 μ m and 20 cm sources which found matches with the other wavelength were 8% and 11% respectively. A flag is set for sources for which there is more than one candidate identification (see below): the selected association is the one with the highest likelihood (Gonzalez-Solares et al 2003).

Radio sources which did not find a 15 μ m match are then interleaved with the matched sources to give an RA-ordered list. Matched sources are given the 15 μ m source name.

We next matched the 6.7 μ m PA sources with the combined 15 μ m-20 cm list, using a search radius of 5''. The larger search radius is required because of the poorer astrometry of the PA catalogue. 30 % of 6.7 μ m sources found a match with a catalogue source.

Non-matched 6.7 μ m sources were associated with optical counterparts where possible, and then interleaved to generate a combined 6.7-15 μ m-20 cm source-list. The positions of all sources in this list which did not have 20 cm fluxes were examined in the ELAIS 20 cm data to see whether a source in the 3-5 σ range might be present, and also in the VLA FIRST survey for areas not surveyed by ELAIS, and

if so the flux was added to the catalogue. Otherwise 3- σ radio limits are given as negative entries in the catalogue.

The 90 and 175 μ m sources were then associated with this combined list using search radii of 30 and 60'' respectively. Where a 90 or 175 μ m source is matched with more than one Catalogue entry, the less probable associations are flagged and are not used in subsequent discussions of infrared colours or spectral energy distributions, ie all the flux is assigned to the most likely match. The non-matched 5- σ 90 and 175 μ m sources were searched for optical counterparts of high likelihood using search radii of 45 and 90'', and the successfully identified sources interleaved into the catalogue. Because of the large positional uncertainties at 90 and 175 μ m, optical counterparts have to be reasonably bright to have a high likelihood of being the correct association ($r < 19.0$). 20 % of 90 μ m sources and 1 % of 175 μ m sources, brighter than 5 σ , found matches neither with the combined 6-7-15 μ m-20 cm source-list nor with optical counterparts. Most of these may be associated with galaxies fainter than $r = 19$. However we can not rule out the possibility that some of the 90 μ m sources may be spurious.

Finally the combined 6.7-15-90-175 μ m-20 cm catalogue is searched for pairs within 5'' and each of these is examined individually. In most, but not all, cases these pairs are believed to be the same object, split in two by the optical association process, and in these case the sources have been merged, with an appropriate flag set in the catalogue.

3.2 Catalogue Description

The final band-merged catalogue is given at <http://astro.imperial.ac.uk/elais/> (available Oct 1st 2003). The catalogue entries are : source name (for merged sources, in order of preference 15 μm , 20 cm, 6.7, 90, 175 μm), source position (same order of preference for merged sources), position of optical association, WFS u, g, r, i, z magnitudes and errors, WFS star/galaxy flags, SExtractor r mag and error, SExtractor star/galaxy classification, positional offset of optical ID (total, RA, Dec), probability of optical association (threshold 0.7), reliability of optical association, 20 cm flux and error, 175 μm flux, error, S/N, positional offset, 90 μm flux, error, S/N, positional offset, 15 μm flux and S/N, 6.7 μm flux and error, 6.7 μm reliability flag (2 = high reliability, 3 = medium reliability), flag 1 (see below), flag 2, J mag and error, H mag and error, K mag and error, flag 3, photometric sed type and redshift ($\lg(1 + z_{\text{phot}})$, derived assuming $A_V = 0$), photometric sed type and redshift and A_V (free fit for A_V), spectroscopic redshift, flag 4, flag5, bolometric optical luminosity L_{opt} , ir sed type (1 = cirr, 2 = M82-sb, 3 = A220-sb, 4 = AGN dust torus, 5 = cooler cirrus, 6 = 2+4), bolometric infrared luminosity L_{ir} , AGN dust torus luminosity L_{tor} (if 15 μm emission is interpreted as due to dust torus emission).

where flag 1 = 1 if radio flux force-merged (15 μm and radio positions within 5"), = 2 if 6.7 μm flux force-merged, = 3 if 90 μm association is not the most likely, where there are multiple associations, = 4 if 175 μm association is not the most likely, where there are multiple associations, = 5 if second-best optical association for 15 μm has been preferred on basis of radio position, = 6 if source has an *IRAS* association, = 7 if 1 and 6 both set, = 8 if 3 and 4 both set, = 9 if 1 and 8 both set, or 4 and 5 both set;

flag 2 = 1 if source falls in gaps between WFS chips, so no optical data, = 2 if source falls near edge of WFS chip, so photometry may be unreliable, = 3 if source has multiple optical counterparts, = 4 if source is blank in optical (ie no optical counterpart with probability of association > 0.7 , within specified search radius), = 6 if there is an association in NED, = 7 if association is bright star, = 8 if flags 1 and 7 set, = 9 if flags 3 and 7 set;

flag 3 = 1 if J,H,K magnitudes from 2MASS, = 2 if J, K magnitudes from Vaisanen et al (2002), = 3 if K magnitudes from Rigopoulou et al (2004, in preparation), = 4 if K magnitude from Pozzi et al (2003);

flag 4 = 1 (spiral) galaxy, = 2 emission-line, starburst, = 3 absorption line, early type, = 4 AGN, = 5 Sy1, = 6 Sy2, = 7 star, = 8 liner;

flag 5 = 1 Perez-Fournon et al (2003), = 2 Serjeant et al (2003), = 3 La Franca et al (2003), = 4 Pozzi et al (2003), = 5 NED, = 6 Morel et al (2001), = 7 SLOAN Survey.

3.3 Associations

We matched the whole catalogue with the NASA Extragalactic Database (NED) and redshifts resulting from these associations are included in our catalogue. We also specifically matched the catalogue to the 2MASS J,H,K catalogues, finding matches for 30 % of our sources (with a preponderance being the stars). Here we discuss some more specific results from associations with known objects.

Table 2 lists the *ISO* and *IRAS* data for ELAIS sources which are associated with *IRAS* Faint Source Catalog sources (FSC, Moshir et al. 1992). Of the 25 associations in N1 and N2, 9 are clearly stellar photospheres detected by *IRAS* at 12 μm (and occasionally at 25 μm) and the rest are nearby normal galaxies. For the 9 stars we can calculate the mean value of $\log_{10}S(12)/S(15)$, which is 0.346 ± 0.03 , compared with an expected value for a Rayleigh-Jeans distribution of 0.20. Since we are reasonably confident of our 15 μm calibration, we infer that the *IRAS* fluxes (in the flux range $100 < S_{12} < 500$ mJy) are too high, by a factor 1.4 on average. This partially accounts for the higher calibration factor (1.75 mJy/ADU) derived by Serjeant et al (2000).

The ELAIS N1 field was also partially observed with the $H\alpha$ survey of Pascual et al. 2001. Since the infrared and $H\alpha$ both trace star-formation it was tempting to see if there were any sources in common. Using the $H\alpha$, FIR, star-formation calibrations of Cram et al. (2001) we were able to estimate a mean $H\alpha$ flux to FIR flux. Then using a starburst SED we were able to estimate the expected 15 μm flux for each of the Pascual et al. sources. With one exception the expected 15 μm fluxes all fell below 1 mJy. The exception was the source in their field a3 with ID 7227b at 16 05 46.3 +54 39 11.74 with $m_I = 17.5$ and $m_{H\alpha} = 17.0$. We estimate that this source should have had a 15 μm flux of 2.9 mJy. Neither this source nor any of the others were detected in our ELAIS catalogue. A more detailed analysis of the expected dispersion in the $H\alpha$ /FIR relation is required before we can assess whether these non-detections suggest that the mean relation needs to be revised.

The Canada-France-Hawaii Telescope blue quasars survey of Crampton et al. 1992 overlaps with the N2 field. 79 of their candidates fall within the ELAIS boundaries. 11 of these candidates are detected by ELAIS and are listed in Table 3.

20-25 % of 15 μm sources (depending on the field) and 75 % of 6.7 μm sources are found to be associated with stars, and the infrared fluxes are consistent with being photospheric emission in almost all cases.

4 RADIO-INFRARED-OPTICAL COLOUR-COLOUR DIAGRAMS

For sources detected in 3 bands we can plot colour-colour diagrams and compare the results with pre-

Table 2. Matches with the IRAS Faint Source Catalog Version 2

IRAS name	12	25	60	100 μ m	sep ($''$)	ELAIS name	6.7	15	90	175 μ m	
F16022+5450	-45.0	-65.7	159.0	-614.0	0.70	ELAISC15-J160322.7+544237	0.00	1.96	101	0.0	
F16029+5506	-66.7	-67.0	296.0	507.0	0.09	ELAISC15-J160408.3+545813	0.00	7.36	315	0.0	
F16046+5415	-83.2	78.8	604.0	798.0	0.25	ELAISC15-J160552.3+540651	0.00	25.33	756	838	
F16063+5405	-69.3	-57.6	244.0	-742.0	0.16	ELAISC15-J160736.5+535730	0.00	16.1	230	597	
F16070+5439	97.5	-50.4	-93.2	-308.0	0.12	ELAISC15-J160812.7+543140	0.00	44.9	0.0	0.0	
F16083+5400	-48.3	-42.6	184.0	-720.0	0.11	ELAISC15-J160934.5+535221	0.00	1.61	215	309	
F16091+5357	207.0	69.9	-102.0	-419.0	0.09	ELAISC15-J161019.2+534934	0.00	87.6	0.0	0.0	
F16091+5447	576.0	146.0	-91.2	7	-244.0	0.02	ELAISC15-J161017.6+543929	0.00	247	0.0	0.0
F16145+5447	-35.7	-64.4	161.0	475.0	0.33	ELAISC15-J161545.8+544020	0.00	17.4	303	0.0	
F16294+4115	-87.8	-65.4	243.0	936.0	0.13	ELAISC7-J163104+410913	2.96	0.00	540	0.0	
F16298+4129	131.0	-53.5	-124.0	-424.0	0.22	ELAISC15-J163130.2+412330	-	55.9	0.0	0.0	
F16323+4127	-74.9	-67.8	383.0	743.0	0.23	ELAISC15-J163401.8+412052	9.60	17.7	403	666	
F16334+4116	-48.4	-65.0	190.0	-813.0	0.17	ELAISC15-J163506.1+411038	0.00	6.9	251	346	
F16337+4101	-66.4	-73.7	224.0	-843.0	0.17	ELAISC15-J163525.1+405542	9.25	12.0	416	682	
F16338+4138	147.0	-70.2	-104.0	-322.0	0.12	ELAISC15-J163531.1+413158	-	90.7	0.0	0.0	
F16341+4053	103.0	-80.2	-88.2	-369.0	0.24	ELAISC15-J163549.0+404720	-	51.1	0.0	0.0	
F16341+4059	243.0	-109.0	-102.0	-339.0	0.10	ELAISC15-J163549.9+405317	0.00	111	0.0	0.0	
F16344+4111	-71.9	-67.6	351.0	897.0	0.06	ELAISC15-J163608.1+410507	2.30	7.74	614	803	
F16349+4038	-84.7	-35.8	236.0	615.0	0.37	ELAISC15-J163633.5+403245	6.15	13.89	291	0.0	
F16349+4034	116.0	-50.7	-98.7	-441.0	0.04	ELAISC15-J163637.3+402824	0.00	41.63	0.0	0.0	
F16359+4058	-61.1	104.0	1220.0	2480.0	0.19	ELAISC15-J163734.4+405208	18.4	45.0	1461	2377	
F16365+4202	-69.6	84.4	460.0	1500.0	0.28	ELAISC15-J163814.0+415620	6.14	42.1	611.0	0.0	
F16377+4150	-54.3	-68.8	306.0	520.0	0.16	ELAISC15-J163923.9+414442	2.55	6.83	299	0.0	
F16389+4146	249.0	81.2	-86.2	-500.0	0.06	ELAISC15-J164033.9+414107	-	106	0.0	0.0	
F16405+4113	-55.6	-68.4	169.0	-545.0	0.15	ELAISC15-J164211.9+410816	1.80	6.98	288	0.0	

Table 3. Quasar candidates from the blue gress survey of Crampton et al. 1992 that are detected by ELAIS. The name of the sources in the Crampton et al catalogue and the ELAIS catalogue are given. This is followed by the separation of the two in arc seconds. The fourth column gives the spectral types estimated from the U, g,r,i,Z INT data in our photometric redshift fitting. The Q flag indicates the confidence of the quasar candidate in the Crampton et al. work from 1 (strong lines) through to 4 (blue continuous spectrum).

Crampton et al. name	ELAIS name	Sep/arc sec	Photo-z	type	Q
1635.20+4124	ELAISC15 J163652.7+411827	1.2		4	2
1635.30+4135	ELAISC15 J163659.0+412928	2.5		6	3
1635.40+4136	ELAISC15 J163702.2+413022	1.1		7	4
1635.70+4121	ELAISC15 J163721.3+411503	0.7		8	3
1636.00+4149	ELAISC15 J163739.3+414348	1.6		7	2
1636.50+4203	ELAISC15 J163805.6+415740	1.4		3	3
1636.70+4133	ELAISR163817+412730	1.3		7	2
1637.20+4217	ELAISC15 J163847.5+421141	0.6		7	4
1637.60+4134	ELAISC15 J163915.9+412834	1.0		6	3
1638.60+4126	ELAISC15 J164016.0+412102	2.5		7	1
1638.70+4108	ELAISC15 J164018.8+410254	1.2		8	3

dictions of models. Figs 3-9 show a selection of these, with predicted loci corresponding to the basic infrared templates used by Rowan-Robinson (2001): cirrus, M82 starburst, Arp220 starburst, AGN dust torus.

Figure 3 shows the 175/90/15 colour-colour diagram for N1 and N2, with loci for cirrus (C), M82 starburst (S), and Arp220 starburst (A), for redshifts from 0 to 6 (the position of the labels indicates the zero redshift end of the loci). The model loci loop around the diagram so without additional redshift information it is hard to say much about the populations (or derive photometric redshifts from far in-

frared data). However from both spectroscopic and photometric redshifts (see section 5) we can deduce that almost all these galaxies have $z < 0.5$. Most of the objects then lie reasonably close to the cirrus locus over this redshift range, so we deduce that this bright subset consists of normal spirals with far infrared emission from interstellar dust bathed in the general stellar radiation field.

Figure 4 shows the 90/15/6.7 colour-colour diagram for N2 and S1, with the same model loci. Again there is ambiguity about the populations involved, which is not resolved using the fact that most galax-

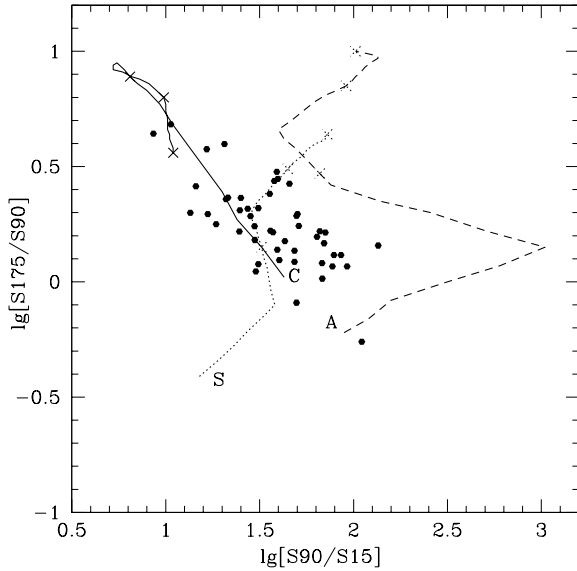


Figure 3. 175-90-15 μm colour-colour diagram for N1 and N2, with loci for cirrus (C), starburst (S) and Arp220 (A) seds, from $z = 0$ to 3 (crosses mark $z = 1, 2, 3$). Only sources detected in all 3 bands are plotted.

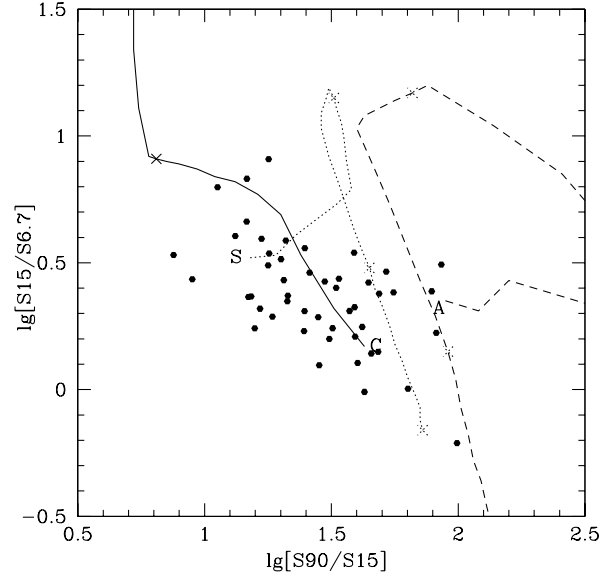


Figure 4. 90-15-6.7 μm colour-colour diagram for N2 and S1, with loci for cirrus (C), starburst (S) and Arp220 (A) seds, from $z = 0$ to 6.

ies detected at 90 μm have $z < 0.5$. An earlier version of this figure was discussed by Marquez et al (2002).

Figure 5 shows the 90/15/r-band colour-colour diagram for N1, with the same model loci. Here the model loci are more differentiated and we can deduce that all three templates are represented, with cirrus and M82 starbursts predominating.

Optical colours provide a powerful discriminant between galaxies and AGN. Many of the catalogue sources in N1 and N2 are detected in each of the WFS band g, r, i. In figure 6 we show the $g - r - i$ colour-colour diagram for sources classified by SExtractor as galaxies. Most of the galaxies define a very tight set of colours, narrower in $(r - i)$ than in $(g - r)$, characteristic of spirals with $0 < z < 0.5$. In figure 7 we show the corresponding plot for objects classified as star-like (excluding actual stars), with different symbols for sources which the photometric redshift code (see section 5) classifies as having AGN-type seds and those with galaxy seds. The AGN occupy quite a tight colour region centred on $(g - r) \sim 0.5$, $(r - i) \sim 0.5$. Objects with galaxy seds show some overlap with Fig 6, but with more scatter to higher values of $(r - i)$, consistent with having higher redshifts.

Figure 8 shows $\lg(S_{15}/S_r)$ versus $(u - r)$ for ELAIS sources, where S_r denotes the r-band flux in mJy. There is a clear separation between the Galactic stars in the lower part of the diagram and the AGN and compact galaxies in the upper part, and between the galaxies and AGN. The objects classified as star-like but with galaxy seds have values of S_{15}/S_r up

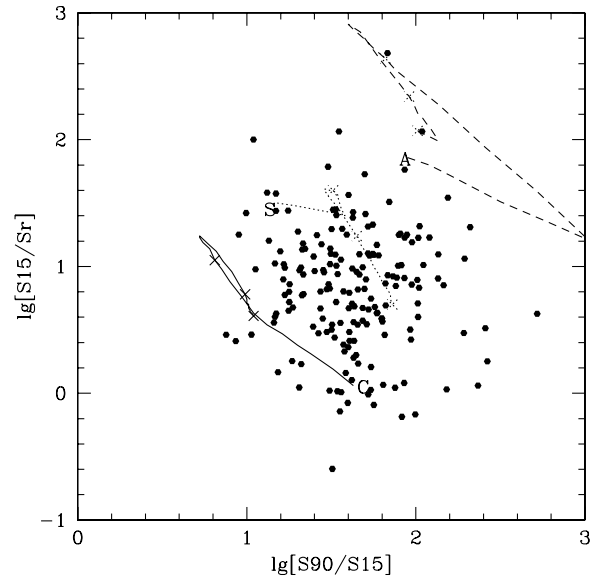


Figure 5. 90-15-r μm colour-colour diagram for N1, N2 and S1, with loci for cirrus (C), starburst (S) and Arp220 (A) seds, from $z = 0$ to 6.

to 300 and these must be heavily obscured starbursts like Arp 220, or Type 2 AGN.

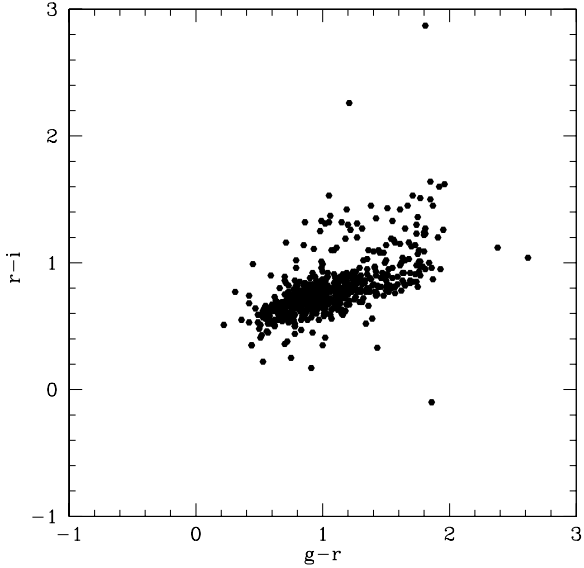


Figure 6. $g - r - i$ colour-colour diagram for galaxies in N1 and N2.

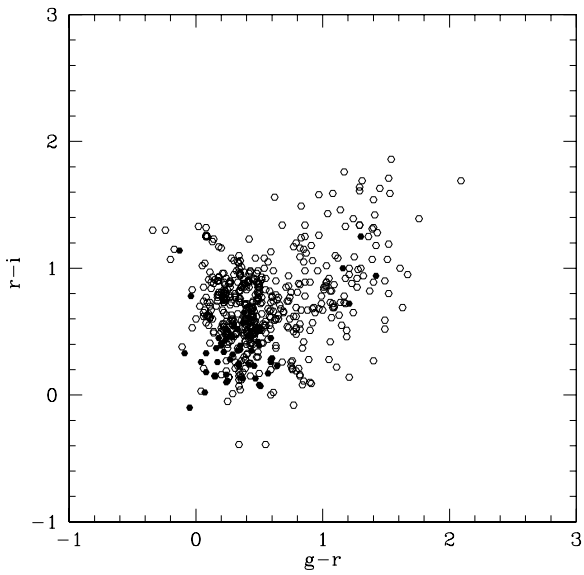


Figure 7. $g - r - i$ colour-colour diagram for star-like objects in N1 and N2. Filled circles: AGN sed, open circles: galaxy sed.

5 PHOTOMETRIC REDSHIFTS IN N1 AND N2

The WFS optical data in the U, g, r, i, Z bands, and J,H,K data (where available) for N1 and N2 allows us to determine photometric redshifts for a large fraction of the sample. The approach used is that of Rowan-Robinson (2003) with a set of 6 galaxy templates, and with the option of varying A_V . In addition two

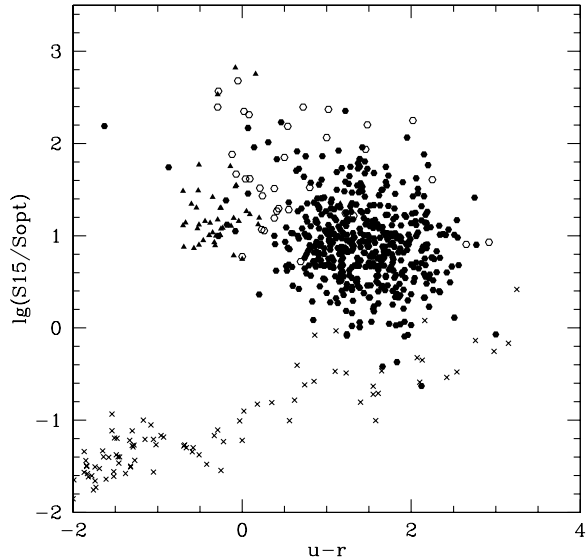


Figure 8. $15/\text{r}$ versus $(u - r)$ for ELAIS galaxies and AGN in N1 and N2. Filled circles: extended optical identifications, filled triangles: star-like objects with AGN sed, open circles: star-like objects with galaxy sed, crosses: Galactic stars.

simple AGN templates are included, based on the average optical QSO spectrum of Rowan-Robinson (1995), modified to take account of observed seds of ELAIS AGN (details of all the templates used are given at <http://astro.ic.ac.uk/~mrr/photz>). The application of this code to the full WFS data set is described by Babbedge et al (2003). We have also used the UBRI data in S2 (Pozzi et al 2003) to estimate photometric redshifts. Figure 9 shows the comparison of photometric and spectroscopic redshifts for N1, N2 and S2. The spectroscopic redshifts in N1 and N2 are reported by Perez-Fournon et al (2003) and Serjeant et al (2003). The agreement is quite good, within the uncertainty of the photometric redshift method ($\sim 10\%$ in $(1 + z)$). The code is quite successful in finding the AGN and estimating their redshifts. Examples of the template fits to optical and near ir data can be seen in Figs 23-25.

Figures 10-13 show redshift histograms at 15, 90 and 175 μm and 20 cm, for sources brighter than the characteristic depth specified in Table 1, with the dotted lines in Figs 10 and 13 indicating spectroscopic redshifts. The broken curve indicates the effect of assigning the 15 μm blank-field sources redshifts evenly distributed in the range 0.5-1.5. The median redshift is 0.2 at 15 μm and 0.1 at 90 and 175 μm .

Figure 14 shows $\lg(S_{15}/S_r)$ versus $\lg(1 + z)$ for objects classified by Sextractor as galaxies, together with predicted loci for cirrus, M82 and Arp220 starbursts. Although most of the galaxies have $z < 0.3$, there are an interesting handful with $0.5 < z < 1$.

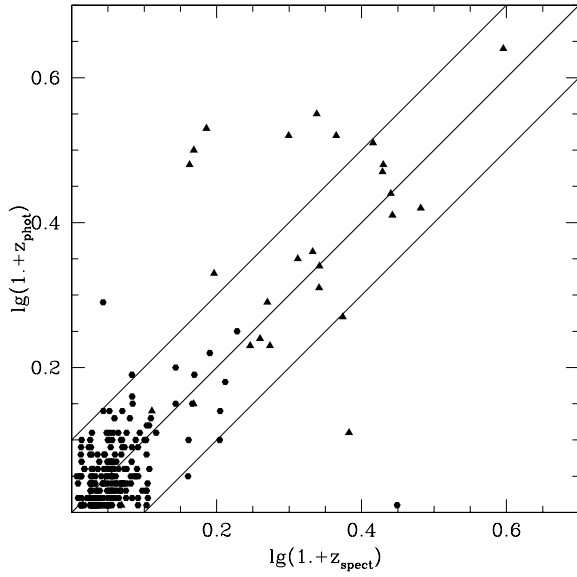


Figure 9. $\lg_{10}(1 + z_{phot})$ versus $\lg_{10}(1 + z_{spect})$. Filled circles: galaxy sed; filled triangles: AGN sed.

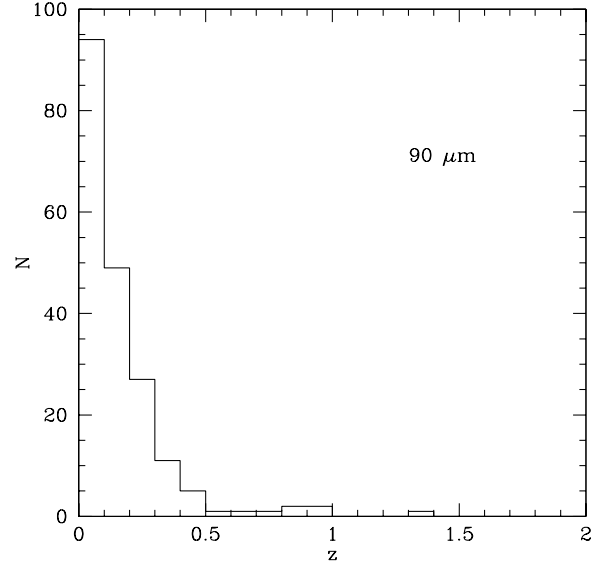


Figure 11. Redshift histogram for ELAIS 90 μm sources. Solid curve: both photometric and spectroscopic redshifts.

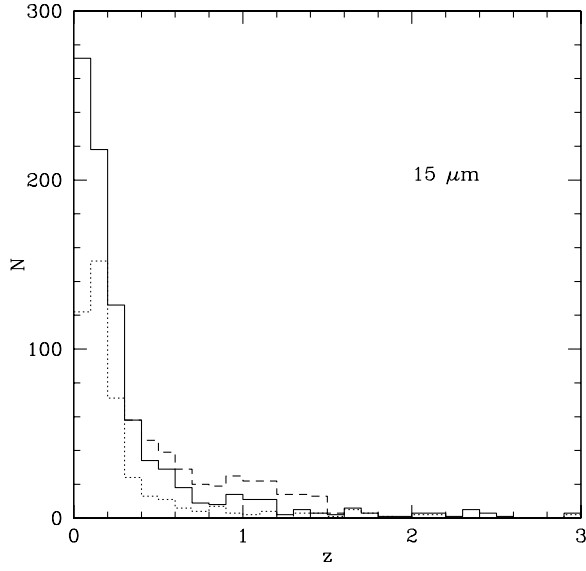


Figure 10. Redshift histogram for ELAIS 15 μm sources. Solid curve: both photometric and spectroscopic redshifts, dotted curve: spectroscopic redshifts only, broken curve: effect of assigning blank fields uniformly to range $0.5 < z < 1.5$.

Figure 15 shows the corresponding diagram for star-like objects, with model loci for AGN dust tori, and M82 and Arp220 starbursts. The objects with AGN sed, shown as filled circles, follow the (Type 1) AGN dust torus model line well. Most with galaxy sed (and some from Fig 14 with $z > 0.2$) have S_{15}/S_{r} values higher than any of the model loci. These may repre-

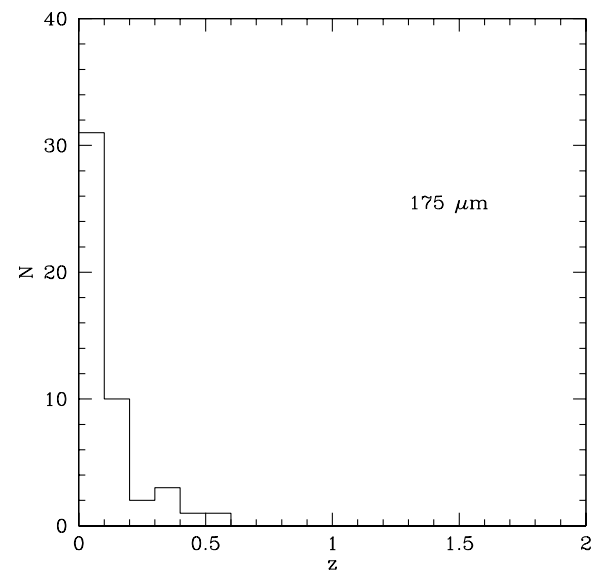


Figure 12. Redshift histogram for ELAIS 175 μm sources. Solid curve: both photometric and spectroscopic redshifts.

sent a new population of heavily obscured starbursts or Type 2 AGN. Fig 16 shows $\lg(S_{15}/S_{20cm})$ versus $\lg(1 + z)$ for all sources: the data are well bracketed by the models, which assume the standard FIR/radio correlation (cf Gruppioni et al 2002). Fig 17 shows $\lg(S_{15}/S_7)$ versus $\lg(1 + z)$ for all sources in N2. Values of $S_{15}/S_{6.7} < 1$ are predominantly stars and have been correctly recognized as such by the photometric redshift code. The 15/6.7 colour ratio is not a

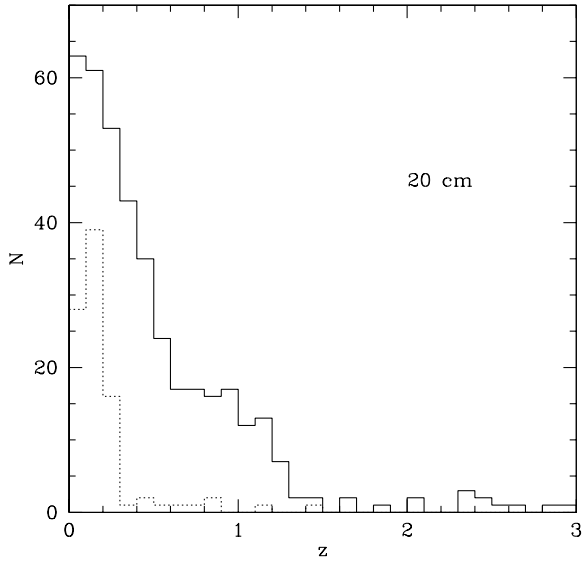


Figure 13. Redshift histogram for ELAIS radio sources. Solid curve: both photometric and spectroscopic redshifts, dotted curve: spectroscopic redshifts only.

good discriminant between the galaxy models at low redshift, though it is clear that at high redshift the sources conform well to the AGN dust torus locus.

Figures 18 and 19 show $\lg(S_{90}/Sr)$ and $\lg(S_{175}/Sr)$ versus $\lg(1+z)$, with model loci for cirrus, M82 and Arp220 starbursts. The models nicely bracket the observational points. However a plot of $\lg(S_{175}/S_{90})$ versus $\lg(1+z)$ (Fig 20) shows that at low redshifts there is a group of nearby galaxies with colder dust than the cirrus template used here.

Figure 21 shows $(g-r)$ versus $\lg_{10}(1+z)$ for objects classified as galaxies, illustrating the strong evolution of $(g-r)$ with redshift. Figure 22 shows the corresponding diagram for star-like objects. The objects with AGN-type sed models follow a narrow locus, those with galaxy sed models occupy a similar region to the galaxies of Fig 21.

6 INFRARED SPECTRAL ENERGY DISTRIBUTIONS

For sources detected in multiple ISO bands we can compare the infrared spectral energy distributions with those for standard model templates. Figure 23 compares the rest-frame sed models of 9 galaxies detected in all four ISO bands with a standard cirrus emission spectrum (Efstathiou and Rowan-Robinson 2003: surface brightness parameter $\psi = 5$, age of starburst = 5 Gyrs). Figure 24 compares 3 galaxies detected in 4 ISO bands and 5 detected in 3 ISO bands with a high optical depth starburst model which gives a good fit to Arp 220 (Efstathiou et al 2000: $A_V = 200$, age of

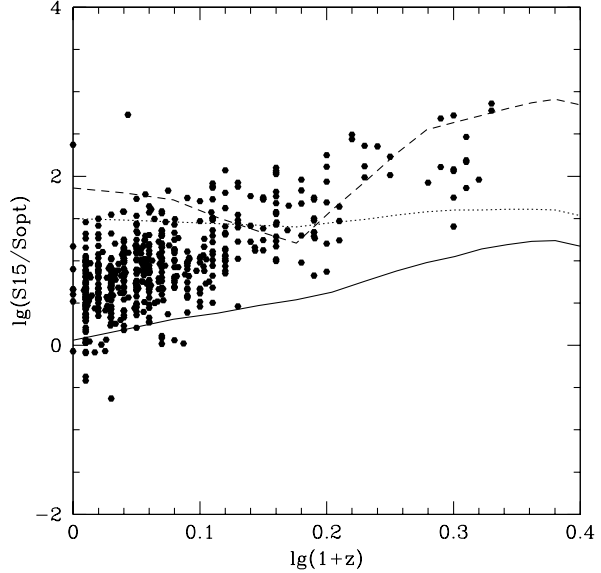


Figure 14. $15\mu\text{m}/r$ -band colour versus $\lg_{10}(1+z)$ for ELAIS galaxies, with loci for cirrus (solid line), starburst (dotted line) and Arp220 (broken line) sed.

starburst = 26 Myr). Figure 25 compares 3 galaxies detected in 3 ISO bands with an M82-type starburst model (Efstathiou and Rowan-Robinson 2001: $A_V = 50$, age of starburst = 26 Myr). Two galaxies for which an AGN dust torus component is also required are included. These figures include all ultraluminous ELAIS galaxies detected in 3 bands ($L_{ir} > 12.22$). The four model components are those used in count models by Rowan-Robinson (2001).

For all ELAIS galaxies detected in two or more bands and with spectroscopic or photometric redshifts (a total of 291 galaxies) we have selected the best-fitting of the four model components cirrus, M82, Arp220 and AGN dust torus, and estimated the bolometric infrared luminosity (from 3-1000 μm : here L denotes the \log_{10} of the luminosity). We have used the $15\mu\text{m}$ flux (or upper limit) to estimate the luminosity in an AGN dust torus component, L_{tor} , if the $15\mu\text{m}$ emission is interpreted as due to such a component (without corroboration at longer wavelengths, L_{tor} gives a more conservative estimate of luminosity than starburst or cirrus models). Estimated the corresponding optical bolometric luminosities (0.04-3 μm), using the photometric sed templates (Rowan-Robinson 2003). Figure 26 shows a plot of $(L_{ir} - L_{opt})$ versus L_{ir} . For ease of comparison with earlier work, and Einstein de Sitter model ($\Omega = 1$, $\Lambda = 0$) model, with $H_0 = 50$, is used.

Galaxies with lower L_{ir} and $L_{ir} - L_{opt} < 0.0$ are predominantly fitted with cirrus models, but cirrus models are also required at higher luminosities and values of $L_{ir} - L_{opt}$ as high as 1.0. This would seem to be consistent with the concept discussed by Efs-

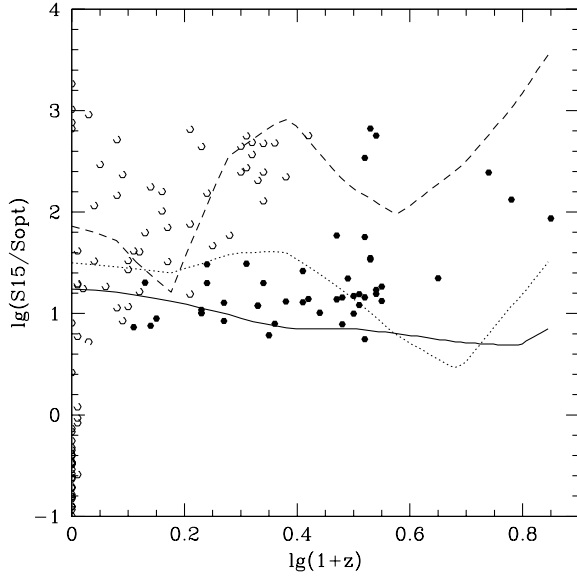


Figure 15. $15\mu\text{m}/r$ -band colour versus $\lg_{10}(1+z)$ for ELAIS star-like sources, with loci for AGN (solid line), starburst (dotted line) and Arp220 (broken line) seds. Filled circles: sources with AGN optical seds, open circles: sources the galaxy seds.

tathiou and Rowan-Robinson (2003) of cirrus galaxies with $1 < A_V < 3$ and high total luminosities, as an alternative explanation of many of the galaxies detected in submm surveys. The expected trend towards M82 and Arp220 -type seds as we go to higher infrared luminosities and higher values of $L_{\text{ir}} - L_{\text{opt}}$ is clearly seen.

Figure 27 shows a similar plot for galaxies for which an AGN dust torus component is preferred. Where galaxies are detected only at 6.7 and 15 μm , and starburst luminosities in the hyperluminous range are implied, we have always preferred a dust torus model as the more conservative assumption. The values of $L_{\text{ir}} - L_{\text{opt}}$ are generally > -1.0 , implying a covering factor $> 10\%$. For values > 0 we must assume that the central AGN suffers some extinction.

7 ULTRALUMINOUS AND HYPERLUMINOUS INFRARED GALAXIES

We have found a surprisingly large population of Arp220-like ultraluminous infrared galaxies ($L_{\text{ir}} > 13.22$) in this survey (10 % of the 15 μm sources). Morel et al (2001) reported the first hyperluminous infrared galaxy in the survey. In fact there are a total of 10 candidate hyperluminous galaxies ($L_{\text{ir}} > 13.22$, Rowan-Robinson 2000) in the survey, listed in Table 4. A further 49 galaxies would be hyperluminous if their 15 μm emission were interpreted as due to a

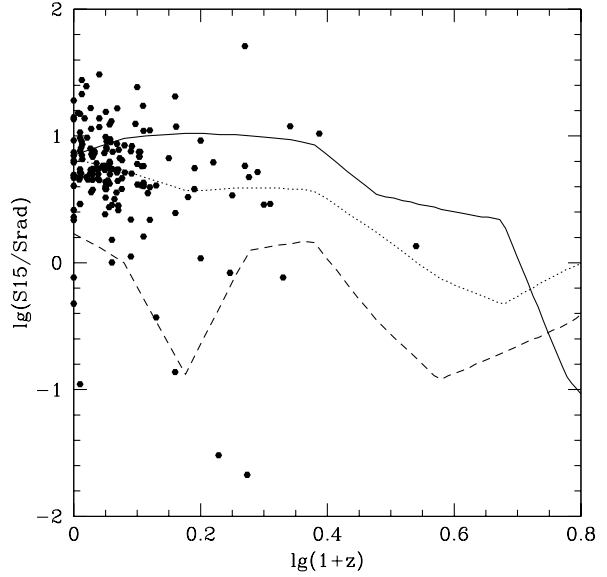


Figure 16. $15\mu\text{m}/20\text{cm}$ colour versus $\lg_{10}(1+z)$ for N1 and N2, with loci for cirrus (solid line), starburst (dotted line) and Arp220 (broken line) seds.

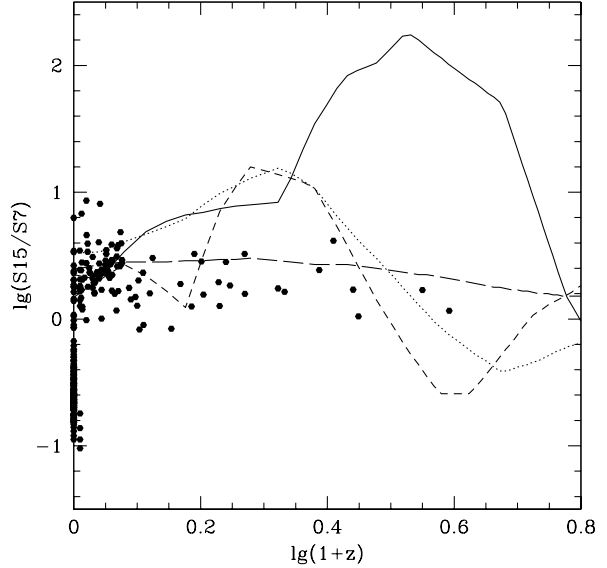


Figure 17. $15/6.7\mu\text{m}$, colour versus $\lg_{10}(1+z)$ for N2 and S1, with loci for cirrus (solid line), starburst (dotted line), Arp220 (short broken line) and AGN dust tori (long broken line) seds.

starburst sed (rather than the more conservative assumption that it is due to AGN dust torus emission). For 6 galaxies this classification is based only on a photometric redshift, and this needs to be confirmed by spectroscopy. The large number of such galaxies is a reflection of the very steep rise in the star-formation

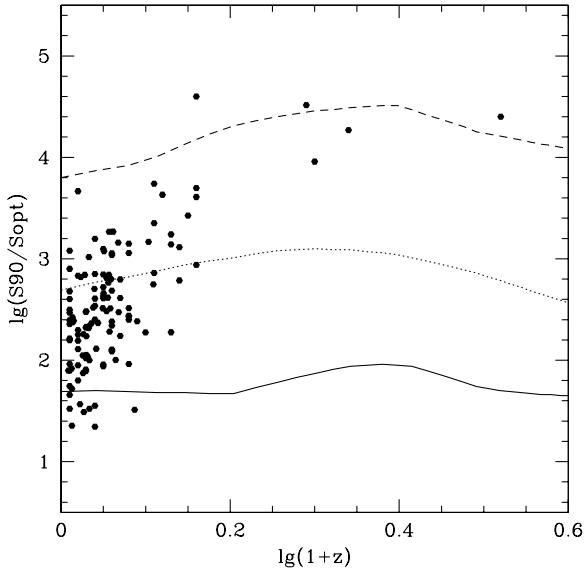


Figure 18. $90 \mu\text{m}/\text{r}$ -band colour versus $\lg_{10}(1+z)$ for ELAIS galaxies, with loci for cirrus (solid line), starburst (dotted line) and Arp220 (broken line) seds.

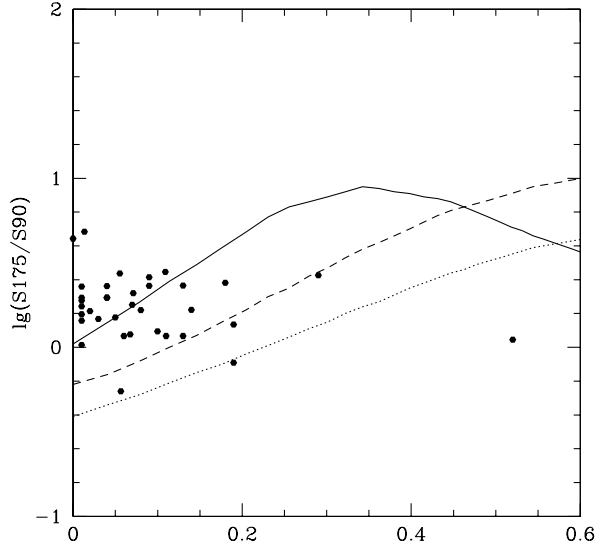


Figure 20. $175/90 \mu\text{m}$, colour versus $\lg_{10}(1+z)$ for galaxies in N1 and N2, with loci for cirrus (solid line), starburst (dotted line) and Arp220 (broken line) seds.

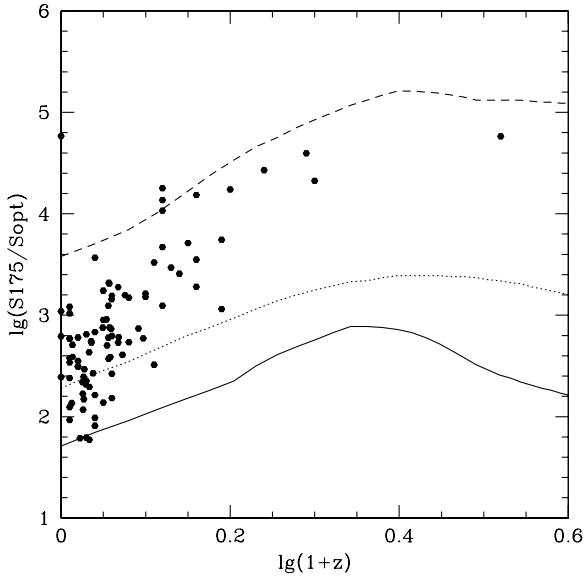


Figure 19. $175\mu\text{m}/\text{r}$ -band colour versus $\lg_{10}(1+z)$ for galaxies in N1 and N2, with loci for cirrus (solid line), starburst (dotted line) and Arp220 (broken line) seds.

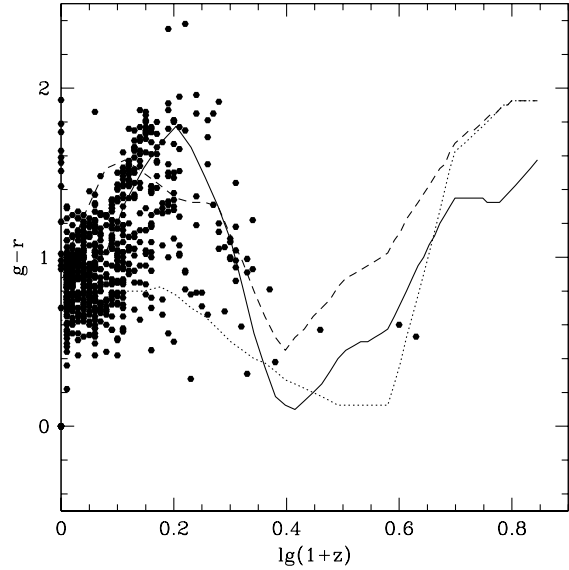


Figure 21. $g-r$ versus $\lg_{10}(1+z)$ for galaxies in N1 and N2. The solid curve is for a cirrus sed, the dotted curve for an M82 starburst, and the broken curve for an Arp220 starburst.

rate between $z = 0$ and $z = 2$, and the associated strong evolution in the AGN population.

We also find 10 ERO's in the survey, defined as $(\text{r}-\text{K}) > 6$, and these are listed in Table 5. 3 of the objects have spectroscopic redshifts and appear to be elliptical galaxies at a redshift ~ 1 .

8 DISCUSSION AND CONCLUSIONS

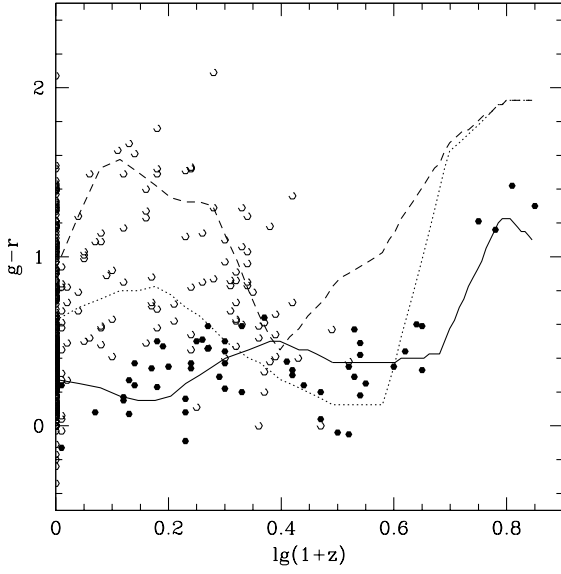
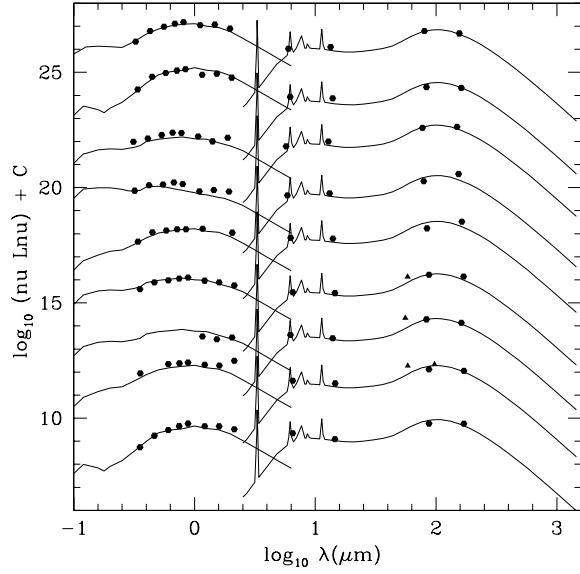
We have presented the Final ELAIS Catalogue at $\text{U}, \text{g}, \text{r}, \text{i}, \text{Z}, \text{J}, \text{H}, \text{K}, 6.7, 15, 90$ and $175 \mu\text{m}$, and 20 cm . The process of band-merging and optical association of the sources has given considerable insight into the extragalactic infrared populations present. Although

Table 4. Hyperluminous infrared galaxies in the ELAIS Catalogue

name	m_r	f_{WFS}	n_{typ}	z_{ph}	z_{spect}	$n_{z,typ}$	$n_{z,ref}$	L_{opt}	n_{ISO}	$n_{ir,typ}$	L_{ir}	L_{tor}
ELAISC15-J160419.0+541524	18.00	0.99	8	2.548	0.000	0	0	13.42	1	2	14.43	13.31
ELAISC15-J160638.0+535009	19.49	0.98	8	3.365	0.000	0	0	13.04	1	3	15.19	13.24
ELAISR 160758+542353	22.70	0.10	8	2.311	0.000	0	0	11.61	2	2	13.80	-12.57
ELAISC15-J161259.2+541505	19.06	0.98	8	2.548	0.000	0	0	12.94	2	1	13.97	12.92
ELAISC15-J163739.2+405643	-	-	0	-	1.438	5	1	0.00	3	2	13.39	12.57
ELAISC15-J164010.1+410521	16.95	1.00	8	1.399	1.0990	0	0	13.40	3	2	13.88	13.12
ELAISC15-J164018.4+405812	18.06	0.99	8	2.311	0.000	0	0	13.33	1	2	14.24	13.22
ELAISC15-J164219.1+412654	22.16	0.29	8	4.495	0.000	0	0	12.39	1	3	15.47	13.52
ELAISC15-J002925-434917	18.63	-	0	-	3.094	5	3	13.59	1	2	14.80	13.54
ELAISC15-J003213-434553	17.09	-	0	-	1.707	5	3	13.57	1	2	14.04	13.29

Table 5. EROs in the ELAIS Catalogue

name	r	K	opt sed	type	z_{ph}
ELAISR16071+544757	24.11	18.076	-	-	-
ELAISC15-J160913.2+542320	24.29	17.180	-	-	-
ELAISR161030+540247	23.53	16.400	-	-	-
ELAISR1046+542329	23.15	17.090	2	1.138	-
ELAISC15-J163536.6+404754	23.38	17.340	1	0.995	-
ELAISR163555+412233	23.29	16.789	1	1.291	-
ELAISR163716+411828	22.64	14.765	-	-	-
ELAISR163723+410526	23.71	17.449	-	-	-
ELAISC15-J163748.1+412100	24.50	17.926	-	-	-
ELAISR163758+411741	23.79	17.413	-	-	-

**Figure 22.** $g - r$ colour versus $\lg_{10}(1 + z)$ for star-like objects in N1 and N2. Filled circles denote objects with AGN sed, open circles objects with galaxy sed. The solid locus is that for the AGN template.**Figure 23.** 9 ELAIS galaxies detected in all 4 ISO bands for which a standard cirrus model provides an excellent fit to the spectral energy distribution. Filled circles: ISO data, filled triangles: IRAS data.

the largest single population is relatively nearby ($z < 0.2$) cirrus galaxies, there is a surprisingly large population of ultraluminous infrared galaxies ($> 10\%$), many of them highly obscured starbursts like Arp 220.

There appear to be a small proportion of genuinely optically blank fields (8 % at 15 μm , 3 % at 6.7 μm , up to 20 % at 90 μm , and 1 % at 175 μm) which must have high infrared-to-optical ratios, be at higher red-

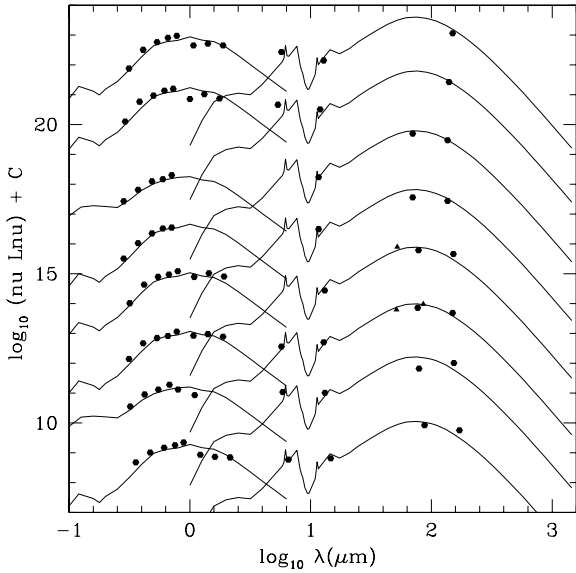


Figure 24. 8 ELAIS galaxies detected in 3 or 4 ISO bands for which an Arp200 model provides an excellent fit to the spectral energy distribution.

shift ($z > 0.2$), and have high infrared luminosities. They are therefore dusty luminous starbursts or Type 2 AGN.

The ELAIS survey provides a strong basis for the SIRTF surveys. The SWIRE Legacy Survey will include the ELAIS N1, N2, and S1 areas. It will be worthwhile to obtain better seds and ir spectroscopy for the luminous infrared galaxies in the survey. As SIRTF does not have a $15 \mu\text{m}$ band, the ELAIS data will be a useful complement to the SWIRE data. The results presented here illustrate the importance of multiband optical data for photometric redshift determination. The far infrared colour-colour diagrams discussed here illustrate the difficulties of trying to determine redshifts from far infrared data alone.

9 ACKNOWLEDGEMENTS

The ELAIS consortium acknowledges support from EC TMR Networks 'ISO Survey' and 'POE', and from PPARC. DMA and OA acknowledge support from the Royal Society.

REFERENCES

- Afonso-Luis A., et al, 2003 (in prep)
- Alezander D.M. et al, 2001
- Babbedge T., et al, 2003 (in prep)
- Babbedge T., 2004, PhD thesis, University of London.
- Basilakos S., et al, 2002, MNRAS 331, 417
- Ciliegi P., McMahon R.G., Miley G., Gruppioni C.,

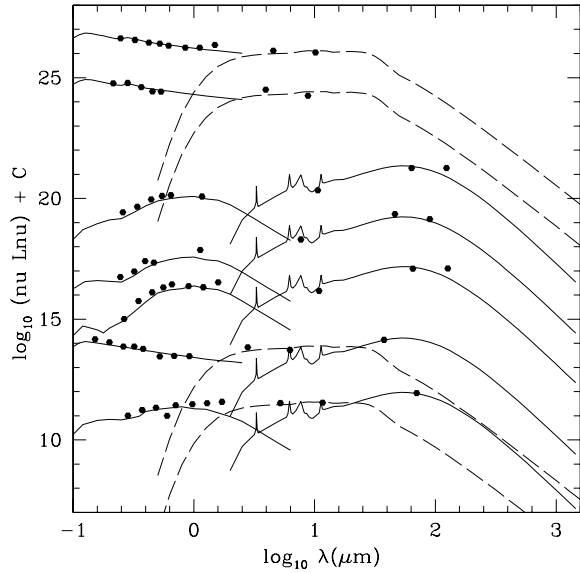


Figure 25. 5 ELAIS galaxies detected in 3 ISO bands compared with an M82 starburst model. For two of the galaxies an AGN dust torus component has been included to fit the mid-ir data (model from Rowan-Robinson 1995). The top two loci are sources identified with quasars, with evidence only for dust torus emission in the infrared.

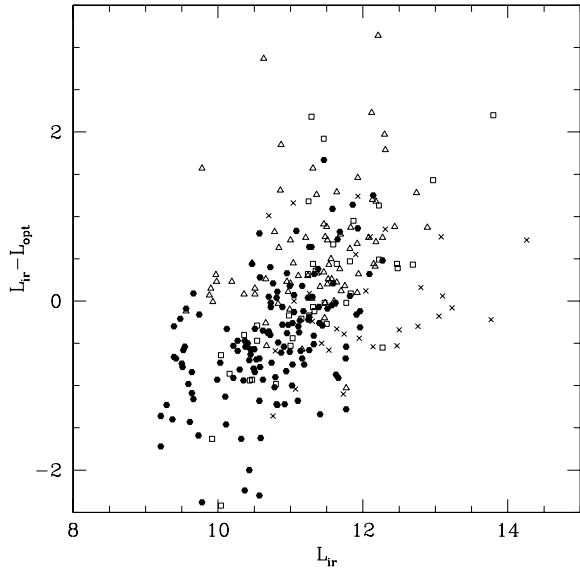


Figure 26. $L_{\text{ir}} - L_{\text{opt}}$ versus L_{ir} for ELAIS galaxies detected in 2 or more ISO bands and with spectroscopic or photometric redshifts. Filled circles: cirrus sed, open squares: M82 starburst, open triangles: Arp 220 starbursts, crosses: M82 starburst+AGN dust torus.

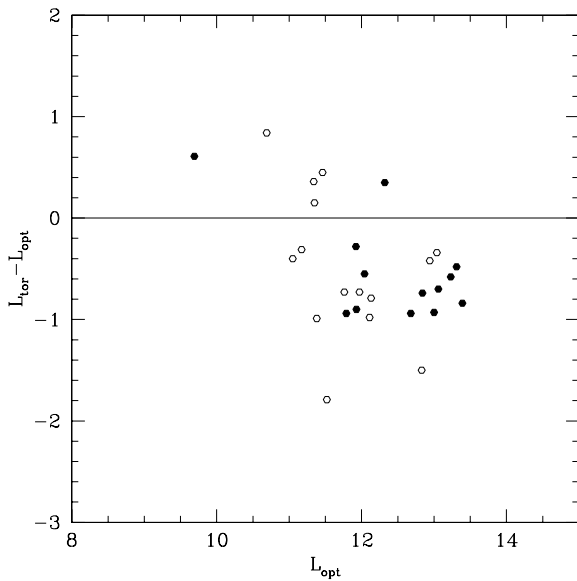


Figure 27. $L_{\text{ir}} - L_{\text{opt}}$ versus L_{ir} for ELAIS AGN dust tori detected in 2 or more ISO bands and with spectroscopic or photometric redshifts. Filled circles: Sy 1 (from optical spectroscopy), open circles: Sy 2, or galaxy sed in optical.

Rowan-Robinson M., Cesarsky C., Danese L., Franceschini A., Genzel R., Lawrence A., Lemke D., Oliver S., Puget J.-L., Rocca-Volmerange B., 1999, MN 302, 222
 Cram et al.
 Crampton D., Cowley A.P., Hartwick F.D.A., Ko P.W. 1992 Astron. J. 104, 1706
 Dole H., Gispert R., Lagache G., Puget J.-L., Bouchet F.R., Cesarsky C., Ciliegi P., Clements D.L., Dennefeld M., Desert F.-X., Elbaz D., Franceschini A., Guiderdoni B., Harwit M., Lemke D., Moorwood A.F.M., Oliver S., Reach W.T., Rowan-Robinson M., Stickel M., 2001, AA 372, 364
 Efstathiou A., Oliver S., Rowan-Robinson M., Surace C., Sumner T., Heraudeau P., Linden-Vornle M.J.D., Rigopoulou D., Serjeant S., Mann R.G., Cesarsky C.J., Danese L., Franceschini A., Genzel R., Lawrence A., Lemke D., McMahon R.G., Miley G., Puget J.-L., Rocca-Volmerange B., 2000, MN 319, 1169
 Efstathiou A., Rowan-Robinson M., Siebenmorgen R., 2000, MN 313, 734
 Efstathiou A. and Rowan-Robinson M., 2003, MN 343, 322
 Gonzalez-Solares E. et al, 2003 (in prep)
 Gruppioni C., Ciliegi P., Rowan-Robinson M., Cram L., Hopkins A., Cesarsky C., Danese L., Franceschini A., Genzel R., Lawrence A., Lemke D., McMahon R.G., Miley G., Oliver S., Puget J.-L., Rocca-Volmerange B., 1999, MN 305, 297
 Gruppioni C., Lari C., Pozzi F., Zamorani G., Franceschini A., Oliver S., Rowan-Robinson M., Serjeant S., 2001, MN 335, 831
 Gruppioni C., Pozzi F., Zamorani G., Ciliegi P., Lari C., Calabrese E., La Franca F., Matute I., 2003, MN (subm)
 Heraudeau P. et al, 2003 (in prep)
 Hughes D.H., Serjeant S., Dunlop J., Rowan-Robinson M.,

Blain A., Mann R.G., Ivison R., Peacock J., Efstathiou A., Gear W., Oliver S., Lawrence A., Longair M., Goldschmidt P., Jenness T., 1998, Nat 394, 241
 La Franca F., et al, 2003 (in prep)
 Lari C., Pozzi F., Frappioni C., Aussel H., Ciliegi P., Danese L., Franceschini A., Oliver S., Rowan-Robinson M., Serjeant S., 2000, MN 325, 1173
 Lari C. et al, 2003 (in prep)
 Lonsdale C. et al, 2003 PASP
 Mann R.G. et al, 2002, MN 332, 549
 Manners et al, 2003,
 Marquez I., Masegosa J., Morel T., Efstathiou A., Verma A., Vaisanen P., Alexander D., Heraudeau P., Surace C., Perez-Fournon I., Cabrera-Guerra F., Gonzalez-Serrano J.I., Gonzalez-Solares E.A., Serjeant S., Oliver S., Rowan-Robinson M., 2000, in 'The Promise of the Herschel Space Observatory', ed G.L.Pilbratt et al, ESA SP-460, p.147
 Matute I., La Franca F., Pozzi F., Gruppioni C., Lari C., Zamorani G., Danese G., Oliver S., Serjeant S., Rowan-Robinson M., 2002, MN 332, L11
 Morel T., Efstathiou A., Marquez I., Masegosa J., Heraudeau P., Surace C., Verma A., Oliver S., Rowan-Robinson M., Georganopoulos I., Farrah D., Alexander D.M., Perez-Fournon I., Cabrera-Guerra F., Gonzalez-Solares E.A., Cabrera-Lavers A., Gonzalez-Serrano I., Ciliegi P., Pozzi F., Willott C.J., Matute I., Flores H., 2001, MN 327, 1187
 Oliver S. et al, 2000, MN 316, 768
 Oliver S. et al, 2002, MN 332, 356
 Pascual S., Gallego J., Aragon-Salamanca A., Zamorano J. 2001, Astron. Astrophys. 379, 798
 Perez-Fournon I. et al, 2003 (in prep)
 Pozzi F., Ciliegi P., Gruppioni C., Lari C., Heraudeau P., Mignoli M., Zamorani G., Calabrese E., Oliver S., Rowan-Robinson M., 2003, MN 343, 1348
 Rowan-Robinson M., Efstathiou A., 1993, MN 263, 675
 Rowan-Robinson M. et al, 1997, MN 289, 490
 Rowan-Robinson M., 2001, ApJ 549, 745
 Rowan-Robinson M., 2003, MN (submitted)
 Serjeant S., Oliver S., Rowan-Robinson M., Crockett H., Misoulis V., Sumner T., Gruppioni C., Mann R.G., Eaton N., Elbaz D., Clements D.L., Baker A., cesarsky C., Danese L., Franceschini A., Genzel R., Lawrence A., Lemke D., McMahon R.G., Miley G., Puget J.-L., Rocca-Volmerange B., 2000, MN 316, 768
 Serjeant S., Efstathiou A., Oliver S., Surace C., Heraudeau P., Linden-Vornle M., Gruppioni C., La Franca F., Rigopoulou D., Morel T., Crockett H., Sumner T., Rowan-Robinson M., Graham M., 2001, MN 322, 262
 Serjeant S. et al, 2003 (in prep)
 Vaccari M. et al, 2003, (in prep)
 Vaisanen P., Rowan-Robinson M., Serjeant S., Oliver S., Morel T., Sumner T., Crockett H., Gruppioni C., Tolstrup E., 2002, MN 337, 1043
 Verma A. et al, 2003 (in prep)
 Willott et al, 2003